

Numerical study of mechanism of diagonal tension failure in reinforced concrete beams

T. Hasegawa

Institute of Technology, Shimizu Corporation, Tokyo, Japan

ABSTRACT: Finite element analysis of diagonal tension failure of reinforced concrete beams is performed using the Multi Equivalent Series Phase Model, and the failure mechanism is discussed by analyzing the numerical results. The first series of analysis shows that in order for diagonal tension failure of the beam to complete the longitudinal splitting crack should propagate unstably, leading to widening and propagation of the diagonal crack. In the subsequent series, a branch-switching analysis is performed to simulate diagonal tension failure of a reinforced concrete beam, assuming that the failure results from a bifurcation starting at a singular (bifurcation or limit) point on the equilibrium path. Adopting the branch-switching method using a scaled corrector, the analysis succeeds in exiting bifurcation modes of failure. But the analysis fails in simulating unstable propagation of diagonal cracks because of stress-locking and crack diffusion, which are typical mesh dependencies in finite element fracture analysis.

Keywords: finite element analysis, Multi Equivalent Series Phase Model, diagonal tension failure, longitudinal splitting crack, diagonal crack, branch-switching analysis, bifurcation, mesh dependency

1 INTRODUCTION

The mechanism of shear failure in reinforced concrete structures is known to be complicated and a number of factors affect it. Especially concerning diagonal tension failure of reinforced concrete beams without shear reinforcement, a lot of experimental as well as numerical research has been carried out to explain the complicated mechanism. However, very few lucid explanations of the failure mechanism have been achieved through numerical research. In this study (Hasegawa 2002a, b, Hasegawa 2003) numerical simulation of diagonal tension failure of reinforced concrete beams is performed using the general purpose finite element system DIANA (Witte & Feenstra 1998), which incorporates the Multi Equivalent Series Phase Model (MESP Model: Hasegawa 1992, Hasegawa 1998). The failure mechanism is discussed by analyzing the numerical results. The Multi Equivalent Series Phase Model is a nonlocal constitutive model derived by treating microscopic fracture regions as series phases consisting of fracture and unloading phases with various orientations. The model has been demonstrated to be able to predict the multiaxial

constitutive relations of concrete materials, which are needed to simulate the fracture of concrete structures (Hasegawa 2001, Hasegawa 2002a, c).

2 ANALYSIS CASES

The diagonal tension failure of reinforced concrete slender beam specimens, BN50 and BN25 (having the same $a/d = 3.0$, but different effective depths d of 450 and 225 mm, respectively) tested at the University of Toronto (Podgorniak-Stanik 1998) is simulated. Both specimens are discretized as finite element mesh types e-1 (Figs. 1, 4) using only cross-diagonal meshes, as well as mesh types e-2 (Fig. 2) and e-3 (Fig. 3) using Delaunay triangulation and cross-diagonal meshes. In this analysis, the mechanism of diagonal tension failure is studied numerically, taking the longitudinal splitting crack at the level of the tension reinforcing bars to be the primary cause of failure as advocated by Chana (Chana 1987). This longitudinal splitting crack is caused by dowel action of the bar, which is primarily influenced by the shear stiffness of the bar. Therefore, to examine the effect of bar shear stiffness on the longitudinal splitting crack,

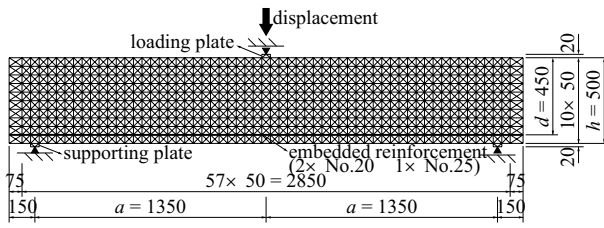


Figure 1. Finite element mesh type e-1 ($d = 450\text{mm}$)

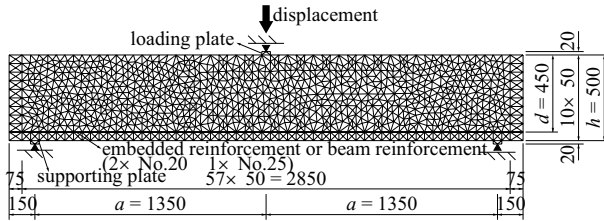


Figure 2. Finite element mesh type e-2

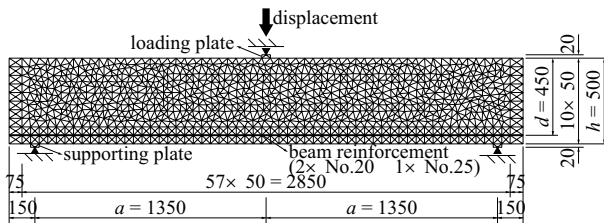


Figure 3. Finite element mesh type e-3

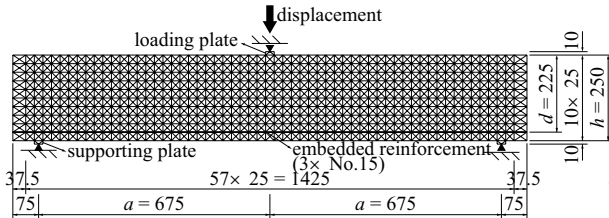
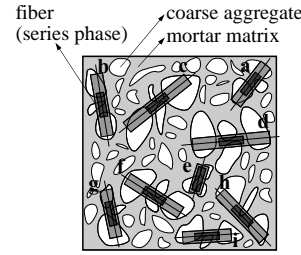


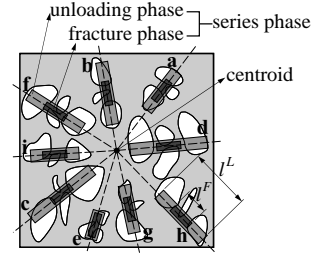
Figure 4. Finite element mesh type e-1 ($d = 225\text{mm}$)

embedded reinforcements (trusses) with no shear stiffness and beam elements are utilized in the analysis. Throughout the analysis, the MESP Model is assumed for all concrete elements.

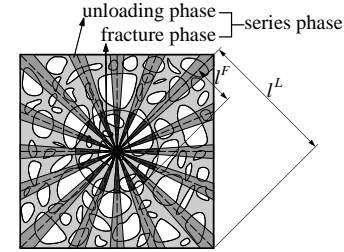
Table 1 summarizes all analysis cases. In analysis cases A, the influence of finite element mesh type and reinforcing bar modeling is examined through basic displacement control analysis at one loading point. On the other hand, in analysis cases B indirect displacement control (de Borst 1986, Rots 1988) is adopted to pass through singular points (limit and bifurcation points) and trace the path after these points that is related to unstable diagonal tension failure. In analysis cases C, two attempts are made to succeed in a branch-switching to bifurcation path leading to unstable diagonal tension failure. Full Newton-Raphson iteration is utilized in all analysis cases.



(a) Random distribution of series phases



(b) Series phases around centroid



(c) Idealized series phases

Figure 5. Fracture, unloading, and series phases in a concrete volume element

3 MULTI EQUIVALENT SERIES PHASE MODEL

The Multi Equivalent Series Phase Model (Hasegawa 1992, Hasegawa 1998) is derived as a nonlocal macroscopic constitutive law to describe size effects due to fracture localization in concrete. Fracture localization at the microscopic level is modeled using a series phase consisting of fracture and unloading phases (Fig. 5). Based on a constant plastic fracture energy law, the stress-strain softening relations of the series phase are converted into those of an equivalent series phase taking into account the length of the series phase. This simple homogenization procedure for the microscopic level yields a regularization of the MESP Model as a nonlocal macroscopic constitutive law. As the load-carrying mechanism of concrete, a number of equivalent series phases are assumed to be distributed with various orientations in the concrete, and the strains in each series phase are kinematically constrained by the macroscopic strain tensor. The resulting incremental stiffness

Table 1. Analysis cases

Analysis case	Finite element mesh type	Reinforcing bar	Calculation method
A1	e-1	embedded reinforcement	displacement control at loading point
A2	e-2	embedded reinforcement	displacement control at loading point
A3	e-2	beam element	displacement control at loading point
A4	e-3	beam element	displacement control at loading point
A5	e-1 ($d=225\text{mm}$)	embedded reinforcement	displacement control at loading point
B1	e-1	embedded reinforcement	indirect displacement control at loading point (arc-length control with spherical path method)
B2	e-1	embedded reinforcement	indirect displacement control for CMOD of longitudinal splitting crack (arc-length control with spherical path method)
C1	e-2	beam element	displacement control at loading point; branch-switching method with scaled corrector
C2	e-2	beam element	displacement control at loading point with small increment

tensor yields an integral formula in terms of orientations of equivalent series phases (Eq. 1);

$$d\sigma_{ij} = C_{ijrs} d\varepsilon_{rs} - d\sigma_{ij}'' \quad (1a)$$

$$C_{ijrs} = \eta \int_{\theta=0}^{\theta=2\pi} \int_{\phi=0}^{\phi=\pi/2} \left[n_i n_j n_r n_s C_N^E + \frac{1}{4} (k_i n_j + k_j n_i) (k_r n_s + k_s n_r) C_{TK}^E + \frac{1}{4} (m_i n_j + m_j n_i) (m_r n_s + m_s n_r) C_{TM}^E \right] \cdot \sin \phi d\phi d\theta \quad (1b)$$

$$d\sigma_{ij}'' = \eta \int_{\theta=0}^{\theta=2\pi} \int_{\phi=0}^{\phi=\pi/2} \left[n_i n_j d\sigma_N^{E''} + \frac{1}{2} (k_i n_j + k_j n_i) d\sigma_{TK}^{E''} + \frac{1}{2} (m_i n_j + m_j n_i) d\sigma_{TM}^{E''} \right] \cdot \sin \phi d\phi d\theta \quad (1c)$$

in which $\eta = \eta^E = 1/(2\pi)$; θ and ϕ = the spherical angular coordinates (Fig. 6); n_i , k_i , and m_i = components of the unit coordinate vectors \mathbf{n} , \mathbf{k} , and \mathbf{m} perpendicular to each other; C_N^E , C_{TK}^E , and C_{TM}^E = incremental elastic stiffnesses for the equivalent series phase; $d\sigma_N^{E''}$, $d\sigma_{TK}^{E''}$, and $d\sigma_{TM}^{E''}$ = inelastic stress increments for the equivalent series phase.

Equation 1 is very similar to that of the Enhanced Microplane Concrete Model (Hasegawa 1995). It has been shown that the model provides good predictions of the experimentally obtained concrete constitutive relations and their size effects.

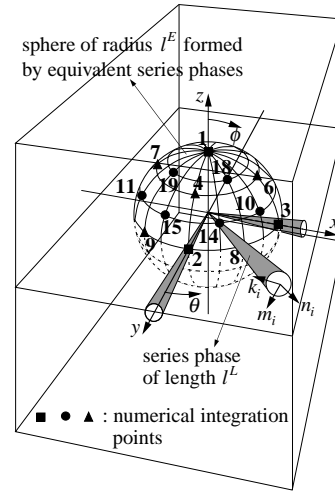


Figure 6. Concrete volume element and sphere

4 ANALYSIS RESULTS AND DISCUSSION

4.1 Analysis cases A

Figure 7 compares the calculated shear response in analysis cases A1, A2, A3, and A4 ($d = 450 \text{ mm}$) with the experiment. Figures 9, 10, and 11 plot the line of maximum principal strain $\varepsilon_1 \geq 5\varepsilon_{t0}$ with thickness proportional to its value. This represents the crack strain and crack direction at maximum shear load V_u in analysis cases A1, A3, and A4, and is a good measure of crack width (ε_{t0} = the tensile strain corresponding to tensile strength). These crack strain figures are compared with the experimental cracking pattern after failure in Figure 8. The incremental deformation just before and at maximum shear load V_u in analysis cases A1, A4 and A5 ($d = 225 \text{ mm}$) is shown in Figures 12, 13, and 14. Shaded areas of localized deformation in the figures indicate cracks with wide openings.

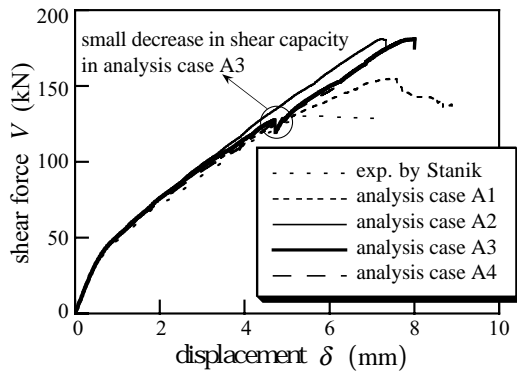


Figure 7. Shear response in analysis cases A

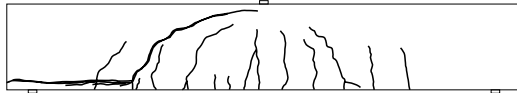


Figure 8. Experimental cracking pattern at failure

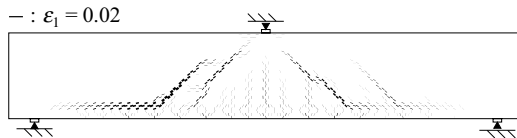


Figure 9. Cracking pattern at V_u (step 659 in analysis case A1)

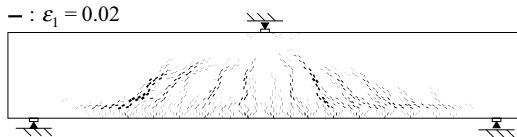


Figure 10. Cracking pattern at V_u (step 708 in analysis case A3)

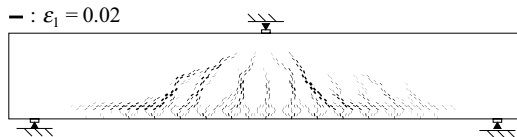


Figure 11. Cracking pattern at V_u (step 586 in analysis case A4)

Analysis case A1 has difficulty in predicting exactly the flatter diagonal crack with curved shape as observed in the experiment, due to the mesh dependency of cracking in the cross-diagonal mesh. The primary diagonal crack widened by a longitudinal splitting crack at the level of the tension reinforcing bars is unable to penetrate up to the loading point since the crack path has a bias due to the cross-diagonal mesh. To complete the collapse mechanism of diagonal tension failure, another diagonal crack needs to propagate further up to the loading point. For this reason overlapping diagonal cracks occur, which increases the shear capacity in analysis case A1, as shown in Figure 7. However, the analysis does reproduce the mechanism of diagonal tension failure as triggered by the longitudinal splitting crack at the level of the tension reinforcing bars (Figs. 8, 9, and 12). In the

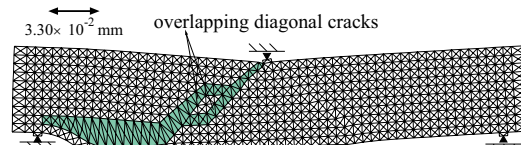


Figure 12. Incremental deformation just before V_u (step 659 in analysis case A1)

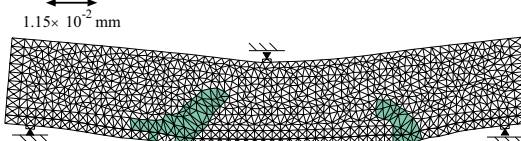


Figure 13. Incremental deformation at V_u (step 586 in analysis case A4)

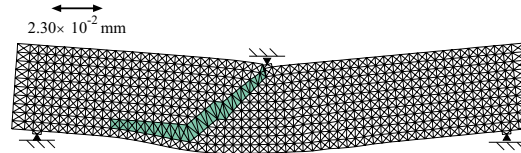


Figure 14. Incremental deformation at V_u (step 280 in analysis case A5)

cross-diagonal mesh, cracks can propagate easily in the direction of element alignment ($\theta = n\pi/4$; $n = 0, 1, 2, 3$), but the shear resistance due to aggregate interlock at cracked elements increases because of the large inclination angle of the cracks. This also causes overestimation of shear strength in analysis case A1, as shown in Figure 7.

The failure to obtain accurate results in analysis case A1 is due to the mesh dependency of cracking in the cross-diagonal mesh. On the other hand, relatively good representation of the cracks is achieved in analysis cases A2, A3, and A4 using the Delaunay triangulation meshes (Figs. 10 and 11). The results are particularly accurate in analysis case A3. When a longitudinal splitting crack at the level of the tension reinforcing bars opens wide and propagates toward the support, a small decrease in shear capacity occurs near the point where the experimental shear load reaches its maximum (Fig. 7). Figures 15 and 16 show the cracking pattern and incremental deformation at the point of this small decrease (at step 375) in shear capacity in analysis case A3. Since the longitudinal splitting crack does not propagate unstably thereafter, the diagonal crack connecting to the longitudinal splitting crack at the level of the tension reinforcing bars neither opens wide nor extends further up to the loading point; consequently, the cracking process fails to reduce to a diagonal tension failure, but results in higher shear capacity and ultimately bending failure. In Figures 17 and 18 show the incremental deformation at the two steps subsequent to step 375,

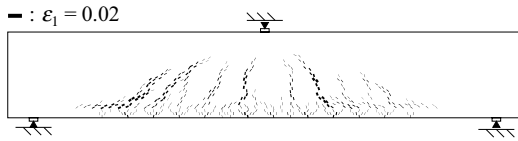


Figure 15. Cracking pattern at point of small decrease in shear capacity (step 375 in analysis case A3)

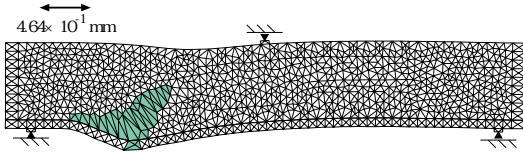


Figure 16. Incremental deformation at point of small decrease in shear capacity (step 375 in analysis case A3)

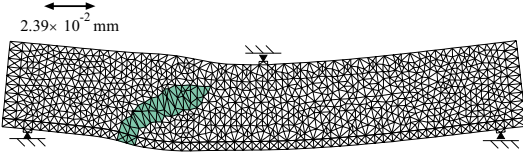


Figure 17. Incremental deformation after the small decrease in shear capacity (step 376 in analysis case A3)

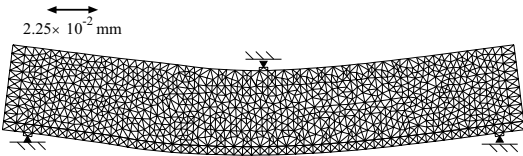


Figure 18. Incremental deformation after the small decrease in shear capacity (step 377 in analysis case A3)

when the small decrease in shear capacity occurred. These figures confirm the above-mentioned cracking process up to bending failure. It should be noted that a careless analysis might be terminated at step 375 without convergence due to the sudden load decrease with unstable propagation of longitudinal splitting and diagonal cracks, mistakenly taking it to represent completion of diagonal tension failure. Although continuation of the analysis is possible beyond step 375, as shown above, if the analysis is continued beyond step 375 it is difficult to simulate further propagation of cracks up to shear collapse. It is important to bear in mind that there might exist a singular point (bifurcation or limit point) in the vicinity of the small decrease in shear capacity. To simulate complete collapse of the reinforced concrete beam due to diagonal tension failure, a branch-switching to bifurcation path for the failure has to be performed using a suitable numerical technique. This will be pursued later in the study.

4.2 Analysis cases B

Figure 19 shows the steps in analysis case A1, at which tangential stiffness matrix \mathbf{K} has negative

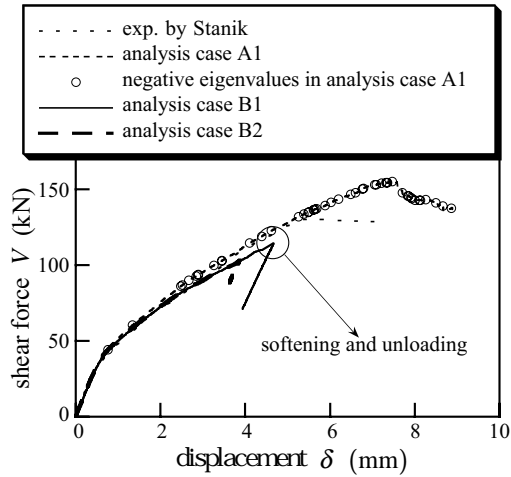


Figure 19. Shear response in analysis cases B

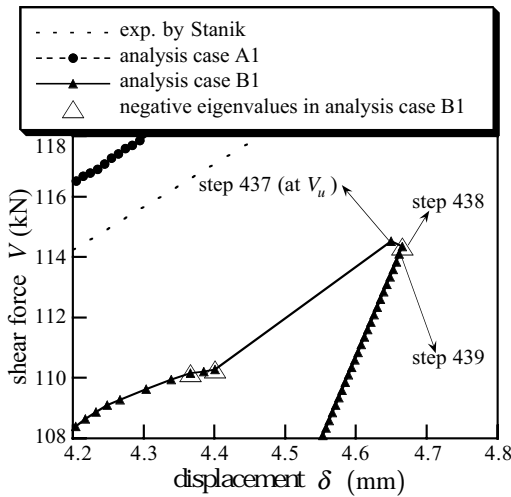


Figure 20. Shear response in analysis case B1

eigenvalues. In the vicinity of the steps along the path at which negative eigenvalues appear, there might exist singular points (limit or bifurcation points) where the determinant of \mathbf{K} becomes zero ($\det(\mathbf{K}) = 0$). In a rigorous branch-switching analysis the singular point is first located, and the eigenproblem is solved to obtain the eigenvalue mode (eigenvector) associated with a zero eigenvalue. Then a scaled eigenvector is applied as a perturbation to the main path, which yields a bifurcation path or post-peak path corresponding to diagonal tension failure. This kind of branch-switching method is well established in geometrically nonlinear problems, especially in post-buckling analysis. However, it is not feasible for such a diagonal tension failure analysis with many singular points along the path. Therefore, in the second series of analysis, i.e., analysis cases B, an indirect displacement control (de Borst 1986, Rots 1988) is used to pass through singular points

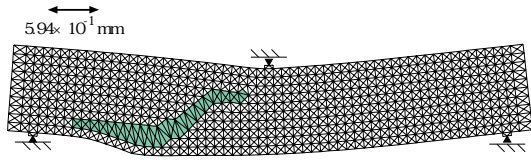


Figure 21. Incremental deformation at V_u (step 437 in analysis case B1)

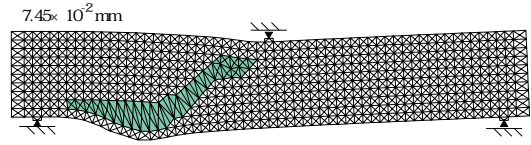


Figure 22. Incremental deformation just after V_u (step 438 in analysis case B1)

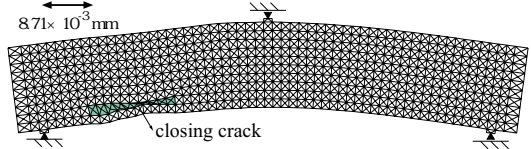


Figure 23. Incremental deformation after V_u (step 439 in analysis case B1)

(limit and bifurcation points) and trace the post-peak path thereafter that is related to unstable diagonal tension failure. This indirect displacement control method does not take into account the existence of singular points, therefore, essentially does not have the purpose of branch-switching. But it is believed to be suitable for passing through the limit point resulting from localized fracture phenomena.

In analysis case B1, a loading point displacement is selected for consideration in a constraint equation for arc-length control with a spherical path method (Witte & Feenstra 1998). On the other hand, in analysis case B2, the CMOD (crack mouth opening displacement) of the longitudinal splitting crack is selected for the purpose. The CMOD of the longitudinal splitting crack is considered to be more suitable for the constraint equation in indirect displacement control than the loading point displacement since the CMOD is more sensitive to fracture localization. However, as shown in Figure 19, the calculation using the CMOD in analysis case B2 results in an unloading path, not a bifurcation path of diagonal tension failure.

As shown in Figure 20, where the shear response around the peak load (step 437) in analysis case B1 is magnified, negative eigenvalues emerge before (step 436) and after (step 438) the peak load. Figures 21, 22, and 23 show the incremental deformation at steps 437, 438, and 439. From these figures it is obvious that indirect displacement control using the loading point displacement happens to succeed in branch-switching to a

bifurcation path of the unstable longitudinal splitting crack and diagonal crack (Figs. 21 and 22). However, as in Figure 22, the diagonal crack is prevented from propagating toward the loading point due to finite element mesh bias (mesh dependency), resulting in widening of the crack tip region. Then at the next step, 439, the softening response that has resulted from the bifurcation eigenvector is not able to continue and an unloading response occurs (Fig. 23). The bifurcation path traced in analysis case B1 does not emerge in analysis case A1, so, shear loading capacity continues to increase, and final shear collapse is reached by diagonal tension failure mode with overlapping cracks (Figs. 9 and 12) as explained before.

4.3 Analysis cases C

Figure 24 shows the steps in analysis case A3 at which tangential stiffness matrix \mathbf{K} has negative eigenvalues. As mentioned in 4.2, in the vicinity of steps with negative eigenvalues there might exist singular points. Branch-switching at a singular point is a promising numerical technique for achieving a bifurcation path or post-peak path corresponding to shear collapse due to diagonal and longitudinal splitting cracks. In analysis case C1, a branch-switching method using a scaled corrector (Noguchi & Hisada 1992) is used to simulate the shear collapse after step 375 of analysis case A3, where the small decrease in shear capacity occurs.

Branch-switching using a scaled corrector is based on the concept that a displacement corrector vector in a full Newton-Raphson iteration can be used in place of the eigenvalue mode usually used for branch-switching, due to the high similarity between the equilibrium equation in full Newton-Raphson iteration and the eigenproblem governing equation at bifurcation points.

At a singular (bifurcation or limit) point where convergence is obtained using full Newton-Raphson iteration, the equilibrium equation is written as

$$\mathbf{K}^{(n)} \Delta \mathbf{u}^{(n+1)} = \mathbf{R}^{(n)} \cong \mathbf{0} \quad (2)$$

in which $\mathbf{K}^{(n)}$ = tangential stiffness matrix at converged iteration n ; $\Delta \mathbf{u}^{(n+1)}$ = displacement corrector vector just after converged iteration n ; $\mathbf{R}^{(n)}$ = out-of-balance force vector at converged iteration n .

On the other hand, the eigenproblem governing equation at a singular point with zero eigenvalue ω_1 is

$$(\mathbf{K}^{(n)} - \omega_1 \mathbf{I}) \phi_1 \cong \mathbf{K}^{(n)} \phi_1 \cong \mathbf{0} \quad (3)$$

in which \mathbf{I} = identity (or unit) matrix; $\phi_1 =$

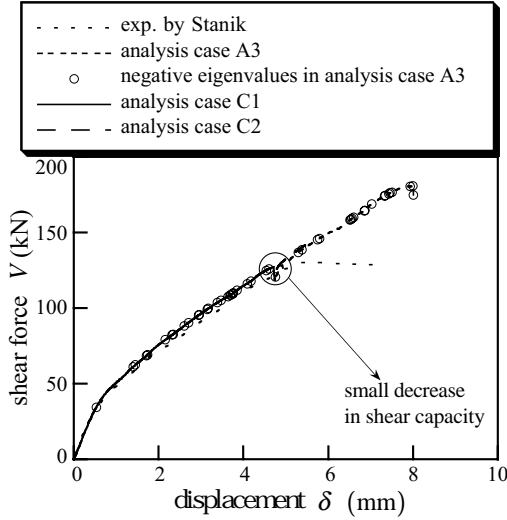


Figure 24. Shear response in analysis cases C

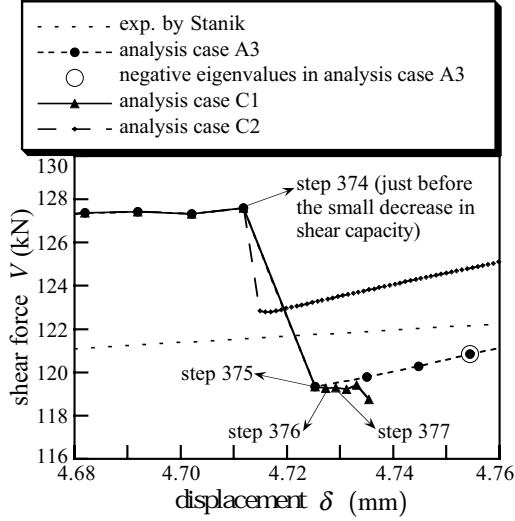


Figure 25. Shear response in analysis cases C

eigenvector corresponding to zero eigenvalue ω_1 . The nearly-equal signs, \cong , mean that Equations 2 and 3 as well as the terms in them have a certain tolerance. Comparing Equations 2 and 3, we have

$$\mathbf{K}^{(n)} \Delta \mathbf{u}^{(n+1)} \cong \mathbf{K}^{(n)} \phi_1 \cong \mathbf{0} \quad (4)$$

This equation suggests that a displacement corrector vector $\Delta \mathbf{u}^{(n+1)}$ just after converged iteration in a full Newton-Raphson iteration can approximate the singular eigenvector corresponding to zero eigenvalue ϕ_1 , i.e.,

$$\phi_1 \cong \Delta \mathbf{u}^{(n+1)} \quad (5)$$

In analysis case C1, a scaled corrector $C \Delta \mathbf{u}^{(n+1)}$ as calculated in Equation 6 is utilized as a perturbation eigenvector ϕ_1 for branch-switching to trace a bifurcation path or post-peak path corresponding to

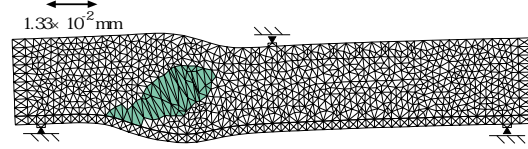


Figure 26. Incremental deformation just after the small decrease in shear capacity (step 376 in analysis case C1)

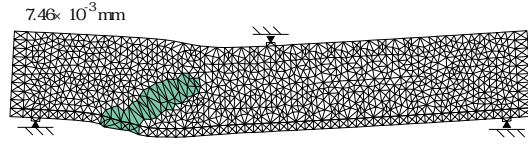


Figure 27. Incremental deformation following the small decrease in shear capacity

shear collapse due to diagonal and longitudinal splitting cracks.

$$C \Delta \mathbf{u}^{(n+1)} = C \cdot (\mathbf{K}^{(n)})^{-1} \mathbf{R}^{(n)} \quad (6)$$

in which C = scaling factor.

Figure 24 shows the shear response in analysis case C1, as obtained by adopting the above-mentioned branch-switching method using a scaled corrector. The resulting bifurcation path from the limit point, step 374, is magnified and shown in Figure 25. Figures 16, 26, and 27 are incremental deformation at steps 375, 376, and 377 along the bifurcation path. When the shear capacity decreases from the limit point of step 374 to step 375, an eigenvalue mode becomes distinguishable, which corresponds to propagation of a longitudinal splitting crack and a diagonal crack connecting to the former crack (Fig. 16). Then at the next step 376, according to the branch-switching method using a scaled corrector, and not updating the tangential stiffness matrix at step 375 but utilizing the stiffness, we succeed in branch-switching to a bifurcation path of unstable propagation of the diagonal crack. As shown for step 376 in Figure 26, this method can recreate unstable propagation of the diagonal crack toward the loading point. However, at the next step, 377, fracture propagation is suppressed as in Figure 27, and divergence occurs in subsequent steps. This suppression of unstable propagation of the diagonal crack is not thought to be due to lack of rigor in implementing the branch-switching method using a scaled corrector, but essentially due to finite element mesh dependencies such as stress-locking (Rots 1988) and crack diffusion, as is obvious from Figures 26 and 27.

In analysis case C2, the usual displacement control at the loading point with small increments after the limit point is adopted to stimulate the bifurcation mode of unstable propagation of

longitudinal splitting and diagonal cracks. The shear response obtained in analysis case C2 is shown in Figures 24 and 25. For several steps following the limit point, the propagation of longitudinal splitting and diagonal cracks induces a very small decrease in shear capacity as in analysis case C1. Then, however, unstable propagation of diagonal crack is suppressed due to finite element mesh dependency, and ultimately a bending mode becomes dominant. This is very similar to analysis case A3 (Figs. 17 and 18).

In this numerical study, dowel action of the tension reinforcing bar is taken into account by the relatively simple means of using beam elements as reinforcing bars. Concerning bond slip behavior between concrete and the tension reinforcing bars this effect is implicitly taken into account through cracking in concrete elements above and below the tension reinforcing bars. However, such models are never sufficient for a rational simulation of diagonal tension failure. A future rational evaluation of diagonal tension failure will depend on predicting local fractures of the concrete at the root of the diagonal crack due to dowel action of the tension reinforcing bars as well as bond slip behavior, which results in the longitudinal splitting crack at the level of the tension reinforcing bars.

5 CONCLUSIONS

Diagonal tension failure of reinforced concrete beams is simulated using the Multi Equivalent Series Phase Model. The analysis provides a lucid explanation of the failure mechanism, and brings certain difficulties and issues related to failure analysis into sharp relief. Analysis cases using cross-diagonal and Delaunay triangulation meshes are both able to reproduce the mechanism of diagonal tension failure as triggered by the longitudinal splitting crack at the level of the tension reinforcing bars. However, analysis cases using a cross-diagonal mesh result in slight overestimates of shear strength due to a mesh dependency that allows cracks to propagate easily in the direction of element alignment. On the other hand, analysis cases using a Delaunay triangulation mesh achieve relatively good representation of the cracks, but unstable diagonal crack propagation and subsequent shear collapse are not obtained since the longitudinal splitting crack connecting to the diagonal crack ceases propagating. Although the loading point displacement or CMOD of the longitudinal splitting crack is selected for consideration in the constraint equation for arc-length control with the spherical path method,

indirect displacement control is not sufficient to pass through the singular points (limit and bifurcation points) and trace the path after these points that is related to unstable diagonal tension failure. Adopting a branch-switching method using a scaled corrector, the analysis succeeds in exiting bifurcation modes of diagonal tension failure. However, the analysis fails in simulating unstable propagation of diagonal cracks because of stress-locking and crack diffusion, which are typical mesh dependencies in finite element fracture analysis.

6 REFERENCES

- de Borst R. 1986. Non-linear analysis of frictional materials. *Ph.D. thesis, Delft University of Technology.*
- Chana, P. S. 1987. Investigation of the mechanism of shear failure of reinforced concrete beams. *Magazine of Concrete Research* 39(141): 196-204.
- Hasegawa, T. 1992. Multi equivalent series phase model for nonlocal constitutive relation of concrete. *Proceedings of the 47th annual conference of JSCE* 5: 18-19 (in Japanese).
- Hasegawa, T. 1995. Enhanced microplane concrete model. In F. H. Wittmann (ed.), *Fracture Mechanics of Concrete Structures*: 857-870. Friburg: AEDIFICATIO Publishers.
- Hasegawa, T. 1998. Multi equivalent series phase model for nonlocal constitutive relations of concrete. In H. Mihashi & K. Rokugo (eds), *Fracture Mechanics of Concrete Structures*: 1043-1054. Friburg: AEDIFICATIO Publishers.
- Hasegawa, T. 2001. Size effect analysis of reinforced concrete deep beams. In R. de Borst, J. Mazars, G. Pijaudier-Cabot, and J. van Mier (eds), *Fracture Mechanics of Concrete Structures*: 689-696. Lisse: Balkema Publishers.
- Hasegawa, T. 2002a. Enhanced microplane concrete model and Multi equivalent series phase model in DIANA for fracture analysis of concrete structures. In M. Hendriks & J. Rots (eds), *Finite Elements in Civil Engineering Applications*: 3-16. Lisse: Balkema Publishers.
- Hasegawa, T. 2002b. Numerical study on diagonal tension failure of reinforced concrete beams. *Proceedings of the 57th annual conference of JSCE* 5: 281-282 (in Japanese).
- Hasegawa, T. 2002c. Size effect analysis of reinforced concrete members using Multi equivalent series phase model. *Proceedings of the 1st fib Congress*: Session 13, 59-68.
- Hasegawa, T. 2003. Branch-switching analysis for diagonal tension failure of reinforced concrete beam. *Proceedings of the 58th annual conference of JSCE* 5: 551-552 (in Japanese).
- Noguchi, H. & Hisada, T. 1992. Development of a new branch-switching algorithm in nonlinear FEM using scaled corrector. *Transactions of JSME (A)* 58(555): 181-188 (in Japanese).
- Podgorniak-Stanik, B. A. 1998. The influence of concrete strength, distribution of longitudinal reinforcement, amount of transverse reinforcement and member size on shear strength of reinforced concrete members. *M.A.S. thesis, University of Toronto.*
- Rots, J. G. 1988. Computational modeling of concrete fracture. *Ph.D. thesis, Delft University of Technology.*
- Witte, F. & Feenstra, P. 1998. *DIANA - Finite element analysis, User's manual*, Release 7. Delft: Building and Construction Research, Netherlands Organization for Applied Scientific Research.